Nanoscale Horizons

ROYAL SOCIETY OF CHEMISTRY

MINIREVIEW

View Article Online
View Journal

Cite this: DOI: 10.1039/d5nh00463b

Surface nanostructures regulated by chalcogen bonding interactions

Xinyi Zhang, [a] Qiang Sun, [a] Liangliang Cai *[ab] and Andrew T. S. Wee *[b]

Received 4th July 2025,
Accepted 5th September 2025

DOI: 10.1039/d5nh00463b

rsc.li/nanoscale-horizons

In recent years, chalcogen bonding (ChB) has emerged as a versatile tool for the bottom-up construction of functional nanostructures on surfaces. This minireview systematically explores the fundamental principles and recent advancements in ChB-directed on-surface synthesis. We highlight how ChB, characterized by its strong directionality and tunable interaction strength, complements conventional noncovalent interactions (hydrogen bonds, halogen bonds, and metal–ligand coordination) in engineering well-defined low-dimensional architectures. The key findings demonstrate ChB's unique capabilities in driving molecular recognition, controlling topology selectivity in conformationally flexible precursors, and facilitating disorder-to-order transitions in two-dimensional (2D) networks. Particularly, we discuss how surface confinement modifies ChB properties, enabling novel assembly pathways and reactivity in on-surface synthesis. By bridging fundamental ChB interactions and the practical implementation in on-surface nanotechnology, this minireview provides valuable insights for designing functional nanomaterials through rational ChB engineering, while outlining current challenges and future directions in this emerging field.

1. Introduction

The construction of well-defined nanostructures on solid surfaces has been a pivotal strategy in nanotechnology, offering unprecedented opportunities for atomic-level control over molecular arrangements and functionalities.[1,2] This surface-confined approach enables the precise engineering of structural parameters and physicochemical properties that are critical for advanced applications.[3–6] The bottom-up fabrication paradigm, particularly through the on-surface molecular self-assembly and on-surface reaction, has allowed the fabrication of complex nanoscale materials and devices with tailored electronic, optical, and catalytic properties.[7–10] The bottom-up

[a] Materials Genome Institute, Shanghai University, 200444, Shanghai, China. E-mail: cailiangliangmgi@shu.edu.cn
[b] Department of Physics, National University of Singapore, 2 Science Drive 3, Singapore 117542. E-mail: phyweets@nus.edu.sg; Web: https://www.physics.nus.edu.sg/~phyweets/

Xinyi Zhang

Xinyi Zhang is pursuing a master's degree at the Materials Genome Institute in Shanghai University under the supervision of Associate Professor Liangliang Cai and Professor Qiang Sun. Over the past year, her research has been focused on on-surface synthesis, especially Ullmann coupling on non-metallic substrates by using UHV-STM, XPS and complementary on-surface science techniques.

Liangliang Cai

Liangliang Cai received her PhD degree in Materials Science and Engineering from Tongji University, China, in 2019 (supervisor: Prof Wei Xu). Thereafter, she was a research fellow in the Department of Physics at the National University of Singapore (NUS), Singapore (supervisor: Prof Andrew Wee). Since 2024, she started working at the Materials Genome Institute, Shanghai University, China, as an associate professor. Her main research interests are on-surface synthesis of low-dimensional nanostructures through scanning probe microscopy and artificial intelligence in surface science including automation of molecular imaging, recognition and manipulation.

approaches leverage the synergistic combination of molecular design principles and intermolecular interactions to achieve structures that cannot be obtained through conventional top-down methods. The resulting low-dimensional nanostructures exhibit remarkable potential for applications ranging from single-molecule electronics and heterogeneous catalysis to biosensing and quantum applications.[11–14] Notably, recent advances in scanning probe microscopy and other surface characterization techniques have further enhanced our understanding and control of these fundamental processes of molecules on surfaces, opening new avenues for the development of functional nanomaterials.[15–17] Particularly promising is the ability to create metastable structures and novel phases that are stabilized by the surface, offering access to nanostructures/nanomaterials with unique characteristics not found in bulk systems.

In the realm of supramolecular self-assembly, researchers have effectively harnessed various noncovalent interactions to construct well-defined nanoscale materials and unconventional organic complexes with atomic precision. Among others, hydrogen bonding has been particularly valuable for creating porous networks with precisely controlled pore sizes and geometries.[18–21] The biological relevance of this interaction is underscored by its crucial role in stabilizing DNA base pairing and protein folding, inspiring the use of biomimetic molecules to construct extended architectures on surfaces.[22,23] Halogen bonding has enabled the creation of complex supramolecular architectures, including the fabrication of molecular Sierpiński triangle fractals.[24–28] These fractal structures, assembled through specific trimeric Br···Br···Br halogen bonding motifs, showcase the precision achievable through noncovalent interactions.[29] The inherent reversibility of these interactions facilitates the growth of large-area and defect-free molecular patterns through enthalpy-driven error correction, which is challenging in the construction of purely covalent interlinking nanostructures.[30]

Andrew T. S. Wee

Prof Andrew Wee is a professor in the Department of Physics at the National University of Singapore (NUS), where he also serves as the Director of the Surface Science Laboratory. His current research focuses on scanning probe microscopy of two-dimensional (2D) materials, heterostructures, and devices as well as on-surface synthesis of molecular nanostructures on surfaces. He is a Fellow and Past President of both the Singapore National Academy of Science (SNAS) and the Institute of Physics Singapore (IPS), and a former Fellow of the Institute of Physics (IoP), UK. He currently serves on the editorial boards of several journals.

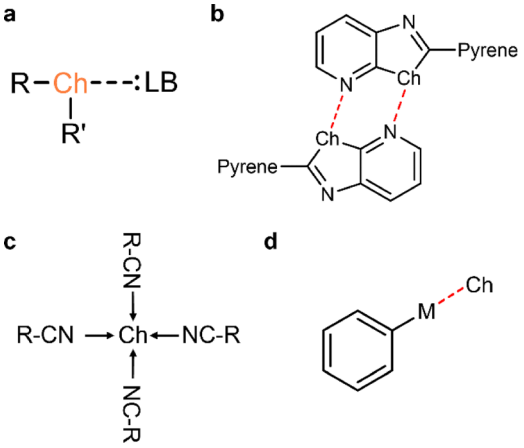

Scheme 1 (a) Schematic representation of a conventionally defined chalcogen bond. (b) Chalcogen bonding interactions explored on Au(111).[43] (c) Chalcogen–organic interaction with the cyano group interacting with a chalcogen atom on Au(111). (d) Carbon–metal–chalcogen interactions on Cu(111).

Transitioning from the supramolecular self-assembly to on-surface reactions, such as the representative Ullmann coupling, precursors undergo elementary steps of dehalogenation, organometallic (OM) formation, and covalent interlinking. Of these steps, the reversible C–M–C organometallic intermediate (where M = Cu, Ag in most cases, and occasionally Au) plays a particularly crucial role in governing both the reaction pathway and the structural outcome of the resulting nanostructures.[5,31–33] The reversibility of these organometallic intermediates is fundamentally important for structural perfection. The involvement of organometallic intermediates has emerged as a key strategy in surface-assisted synthesis, where their lifetime and stability can be modulated through careful selection of metal substrates and reaction conditions, such as atomic doping.[34,35]

While these conventional secondary bonding interactions (SBIs) continue to dominate constructing noncovalent carbon nanostructures, the emerging potential of chalcogen bonding interactions (ChBIs) – involving the group VIA elements such as selenium (Se), and tellurium (Te) – has recently garnered a notable surge of attention to foster the construction of well-defined nanoscale materials due to their chemical versatility.[36,37] ChB originates from the anisotropic charge distribution around chalcogen atoms (S, Se, and Te), whereby covalent bonding to electron-withdrawing substituents generates an electron-deficient region known as the σ-hole along the extension of the covalent bond axis.[38,39] This σ-hole can attractively interact with electron-rich sites such as lone pairs or π-systems (as shown in Scheme 1a), giving rise to interactions that are not only comparable in strength and predictability to hydrogen and halogen bonds but are also strongly directional, as the σ-hole is localized along the bond axis, enforcing near-linear donor–acceptor geometries.[40,41] These distinct advantages, such as tunable strength, directionality, and compatibility with diverse molecular backbones, render ChB particularly suitable for engineering well-defined

nanostructures on surfaces. Recent studies have demonstrated that ChB can drive the formation of highly ordered supramolecular frameworks and 2D networks even from conformationally flexible precursors (as depicted in Schemes 1b–d).[42–46] As "unusual" SBIs, ChBIs not only complement existing noncovalent interactions in hybrid systems but also induce controllable structural transformations through external stimuli, thus having the potential to template the growth of metal organic frameworks (MOFs) and facilitate charge transport in organic-based electronic applications.

ChB has been relatively underexplored over the last few decades, but recent years have witnessed a steady increase in interest regarding its applications, especially in crystal engineering and in solution.[47,48] In addition, growing attention has also been devoted to supramolecular assemblies, where ChB has been demonstrated to direct chiral self-assembly and complex architectures.[36,49] ChB has been reviewed from different perspectives before, so here in this minireview, we will not cover the topic comprehensively but will only highlight recent advances in ChB-mediated surface nanostructures, focusing on design principles, structural characterization, and potential applications. We conclude with an outlook on emerging opportunities and current challenges in harnessing ChB for applications in advancing surface nanostructures. By bridging the gap between fundamental ChBIs and their practical implementation in surface nanotechnology, this minireview aims to provide new perspectives for designing functional nanomaterials through rational ChBI engineering, and enrich the toolkit of bottom-up fabrications.

2. Molecular self-assembly driven by chalcogen bonding

ChB arises from the ambiphilic nature of chalcogen atoms (S, Se, and Te), where the electrophilic σ-hole interacts with Lewis bases (N, O, π-systems, *etc.*), while the nucleophilic lone pairs retain conventional bonding. This dual character enables unique orthogonal interaction networks, though the electrophilic component remains underexploited in supramolecular design.[50–52]

Over the past few decades, noncovalent interactions including hydrogen bonding, metal coordination and dipole–dipole interactions have been extensively employed in molecular self-assembly on surfaces, enabling precise construction of low-dimensional nanostructures. However, ChB, which has been widely employed to create ordered noncovalent assemblies in bulk crystals and liquids, still remained systematically underexplored in surface-confined molecular assembly.[53–56] Among recent advances in understanding ChB mechanisms, two seminal studies have established ChB as a viable paradigm for on-surface molecular engineering.[43,44] Camilli *et al.* achieved the first demonstration of ChB-driven chiral dimerization on Au(111), by designing Te/Se-containing pyridine derivatives.[43] Complementarily, Zheng *et al.* constructed a two-dimensional molecular network with 4-fold symmetry on Au(111) through Te–carbonitrile interactions.[44]

These studies could not only establish ChB as a viable strategy for constructing two-dimensional functional architectures but also expand the toolbox of noncovalent interactions for on-surface crystal engineering.

2.1. On-surface supramolecular dimerization driven by chalcogen bonding

To demonstrate the experimental evidence of on-surface molecular self-assembly driven solely by ChBIs, Camilli *et al.* engineered chalcogenazolo-pyridine (CGP) derivatives to achieve supramolecular dimerization on Au(111) through directional Ch···N interactions. The molecules CGP–Te and CGP–Se provide the directional Te···N and Se···N chalcogen bonds. As illustrated in Fig. 1a, CGP–Te exhibits the existence of chiral dimers with two enantiomers.

Scanning tunnelling microscopy (STM) images in Fig. 1b revealed that CGP–Te and CGP–Se molecules self-assembled into dimeric architectures on the Au(111) surface, exhibiting distinct six-fold rotational symmetry. In stark contrast, the benzo-Te molecules lacking the pyridyl moiety failed to form well-defined assemblies, resulting in disordered aggregates. This result thereby underscored the critical role of Ch···N interactions in surface-confined molecular recognition.

The detailed molecular backbone of the $(CGP–Te)_2$ dimer, resolving the pyrene cores and the terminal chalcogen atoms, was disclosed through bond-resolved STM (BRSTM) images (Fig. 1c). The corresponding density functional theory (DFT)

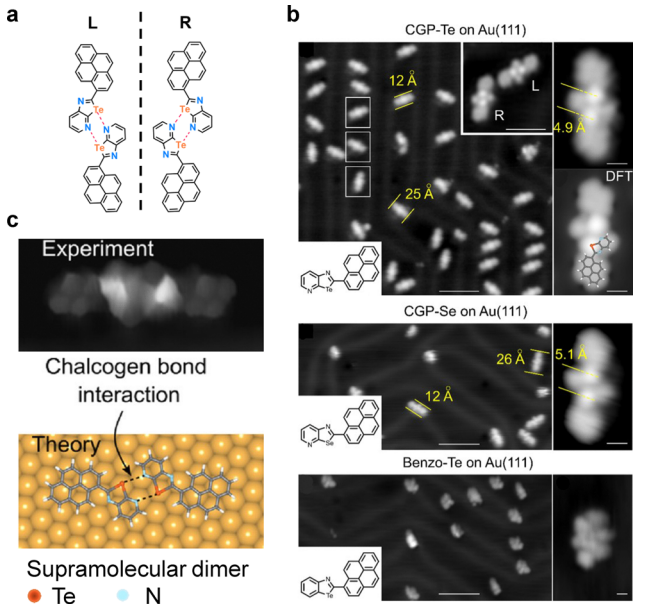

Fig. 1 (a) Schematic representation of the chiral $(CGP–Te)_2$ dimer. (b) Large-scale and high-resolution STM images of the $(CGP–Te)_2$ dimer, $(CGP–Se)_2$ dimer, and the reference tellurazole molecule on Au(111), with the corresponding molecular schematics indicated. (c) Bond-resolved STM image and the DFT relaxed geometrical model of the individual $(CGP–Te)_2$ dimer. Reproduced from ref. 43. Copyright 2024 American Chemical Society.

optimized geometry further confirmed the proposed dimeric structure and validated the assignment of the bright BRSTM features to the Te centers. The agreement between experimental and theoretical data (the distances of Te···Te and Te···N) provides strong evidence that the observed assemblies are stabilized by ChB. Consequently, the ability of ChB to precisely direct the assembly of chiral supramolecular dimers on surfaces has been confirmed.

Importantly, the computed values reported that the interaction energies of $(CGP–Te)_2$ and $(CGP–Se)_2$ dimers in the gas phase are −9.2 and −6.2 kcal mol^{-1}, respectively. When adsorbed on Au(111), the interaction energy values are calculated to be −5.7 kcal mol^{-1} for $(CGP–Te)_2$ and −3.9 kcal mol^{-1} for $(CGP–Se)_2$ dimers, suggesting that the dimer formation remains favorable, although weak.[43] In contrast, the reference benzo-Te system lacking the pyridyl acceptor group indicates a destabilizing interaction energy of +1.1 kcal mol^{-1}, consistent with the absence of dimer formation in experiments. These values confirm that ChB is sufficiently strong to stabilize ordered supramolecular dimers, even under surface confinement. Energy decomposition analysis of other studied ChB systems[57] further elucidated the dual nature of ChB, with electrostatic contributions up to 58%[58] in chalcogenadiazole dimers, while orbital mixing components can be as high as 41% in telluradiazoles.[59] This underscores the unique combination of strength and directionality, distinguishing it from other noncovalent interactions in the engineering of 2D molecular architectures.

2.2. Construction of molecular networks *via* tellurium-based chalcogen interactions

Zheng *et al.* explored the formation of Te-mediated molecular self-assembly on a metal surface,[44] where a carbonitrile molecule (shortened as TdCN and shown in Fig. 2b) interacts with Te atoms to form chalcogen–organic interactions. As depicted in Fig. 2a, the structural model consists of a single tellurium (Te) atom that interacts with four TdCN molecules through cyano groups.

In the absence of Te atoms, TdCN assembles into close-packed nanostructures on Au(111) as displayed in the STM images of Fig. 2b. Subsequent deposition of Te atoms onto the TdCN-covered Au(111) surface maintained at room temperature

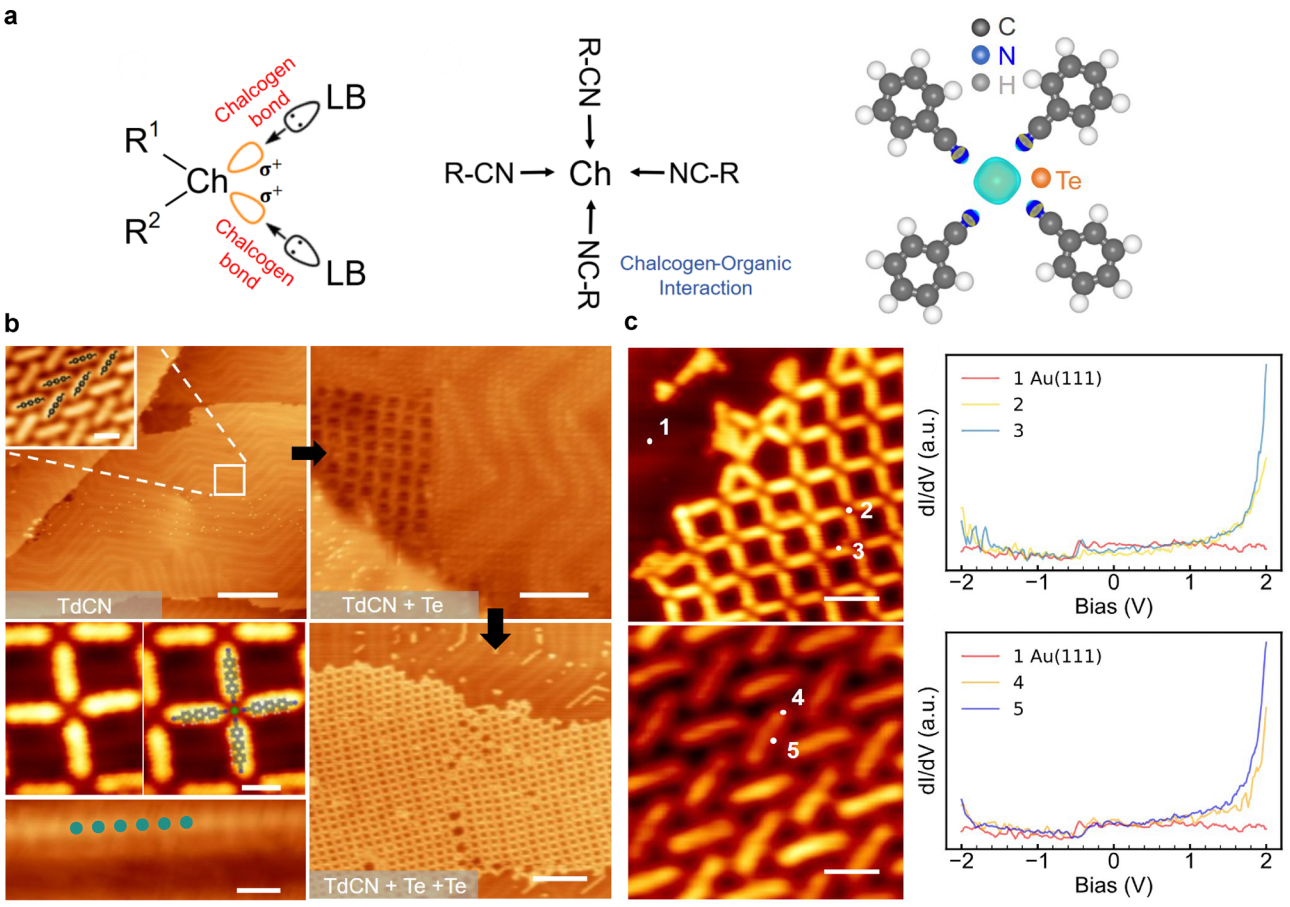

Fig. 2 (a) Schematic representations of conventionally defined chalcogen bonds and the chalcogen–organic interaction with four cyano groups interacting with a chalcogen atom (Te). (b) STM images of Te-directed self-assembled phase formed after deposition of precursor TdCN on Au(111), followed by addition of Te step-by-step. The zoomed-in STM images indicate the 4-fold interacting motif with the superimposed structural model, and the Te atoms are highlighted by green dots. (c) STS measurements on the Te-directed molecular network and the pristine close-packed nanostructure composed of sole TdCN molecules. Reproduced from ref. 44. Copyright 2024 American Chemical Society.

(RT) led to a transformation in the molecular pattern, forming a square molecular network characterized by a 4-fold binding motif. This structural evolution was attributed to the Te–carbonitrile interactions which served as the driving force for the self-assembly process. After further deposition of Te atoms on the sample, the pristine close-packed structures completely converted to square networks. The zoomed-in STM images provide a detailed view of the 4-fold interacting motif and the Te chain (Fig. 2b).

The authors carried out careful DFT calculations to elucidate the nature of the Te–carbonitrile interaction. The binding energy of the Te-directed 4-fold motif was approximately 0.265 eV ($\sim$6.1 kcal mol^{-1}) per molecule which is comparable to medium-strength hydrogen bonding (typically 4 to 15 kcal mol^{-1})[60] but weaker than typical metal–organic coordination bonds such as Cu–N (15 to 31 kcal mol^{-1}).[61] In comparison, halogen bonding interactions (*e.g.*, Br$\cdots$N or Br$\cdots$Br) generally fall in the range of 2 to 7 kcal mol^{-1},[38,62] while van der Waals interactions are usually $<$2 kcal mol^{-1} and lack intrinsic directionality.[63–65] These quantitative comparisons highlight that ChB is weaker than transition metal coordination but sufficiently strong and directional to rival hydrogen and halogen bonding, thereby enabling controllable on-surface self-assembly.

Charge density difference analysis indicated directional charge transfer between Te and the cyano groups, stabilizing the network through electrostatic interactions. Notably, the Te atom was positioned below the molecular plane due to its interaction with the Au(111) substrate. As confirmed by Bader charge analysis, the molecule–substrate interaction is attributed to charge transfer between Te and the molecules, and compared it to that in the gas phase. Scanning tunneling spectroscopy (STS), present in Fig. 2c, exhibited identical dI/dV spectra for TdCN molecules in both the Te-directed networks (site 3) and pristine close-packed structures (sites 4 and 5), with characteristic HOMO ($-$1.8 V) and LUMO (1.6 V) resonances preserved, which confirmed that the Te-directed assembly preserved the intrinsic electronic properties of the pristine TdCN molecule.

9wMoreover, further experiments incorporating Cu atoms into the Te–TdCN system revealed complete replacement of Te–carbonitrile networks by Cu-directed linear chains, demonstrating the comparatively weaker binding strength of Te relative to transition metals. Although Te-directed assemblies exhibit kinetic favorability at RT, they gradually degrade over time, reverting to close-packed structures and highlighting their inherent thermodynamic instability. In general, the authors revealed atomic-scale insights into the nature of the chalcogen–organic interaction on the metal surface, establishing a foundational framework for designing and modulating low-dimensional nanostructures.

3. Organometallic networks regulated by C–M–Ch bonding

In their work,[45,46] Cai *et al.* have demonstrated that Se enables the formation of more ordered crystalline phases through co-deposition with the conformationally flexible precursors, which greatly improved the OM structural homogeneity. This work has uncovered the ability of Se doping to achieve topology selectivity of a conformationally flexible precursor.[45] The subsequent study further revealed the disorder–order transition of 2D molecular networks by Se doping.[46] From the mechanism point of view, the Ullmann coupling reaction facilitates precursor debromination to form OM intermediates,[66] while Se adatoms stabilize specific ordered architectures by modulating energy landscapes *via* C–Cu$\cdots$Se interactions.

3.1. Topology selectivity through selenium doping

Previous literature studies suggest that Se doping exhibits modulatory effects on self-assembly and crystallization behaviour.[67–70] Herein Cai *et al.* explored the low coverage ($\sim$0.01 ML) Se doping with the conformationally flexible precursor 2,4,6-tris(3-bromophenyl)-1,3,5-triazine (*m*TBPT) on the Cu(111) substrate and achieved high topology selectivity as shown in Fig. 3a. The conformationally flexible *m*TBPT with two conformers C_{3h} and C_s becomes chiral upon 2D confinement, which increases the complexity of control in the topology selectivity and nanostructure uniformity.

Without Se deposition, after annealing at 365 K, the random phase formed by completely debrominated *m*TBPT was obtained on Cu(111), with stochastic distribution of molecular conformations confirmed by high-resolution STM imaging depicted in Fig. 3b. Statistical analysis of 1200 molecules demonstrated the absence of topology selectivity, as evidenced by the formation of the random C–Cu–C OM nanostructure.

Remarkably, the selectivity of the C_{3h} conformer was greatly improved after co-deposition of 0.28 ML *m*TBPT and 0.01 ML Se on Cu(111) at 365 K, facilitating the selective formation of C_{3h}-based OM networks with highly ordered 2D nanoporous networks as shown in Fig. 3c. The close-up STM image shows that the (*L*) and (*R*) domains deviated 15 $\pm$ 3° from the [011] direction of the substrate. Statistical analysis reveals approximately 90% selectivity for the C_{3h} conformer, excluding undeterminable periphery moieties of the networks (close to 10%). Additionally, the selectivity remains invariant regardless of the deposition sequence of *m*TBPT and Se. The disorder-to-order transition of phases has been reproducibly achieved through post-deposition exposure of the random phase to Se adatoms at RT for enough time (*i.e.* overnight), establishing a robust strategy for topological control. Kinetic control enables the proportion of hexagonal OM rings to increase through either thermal activation (365 K) or prolonged mild annealing (RT for overnight).

The mechanism of Se doping-induced conformational transformation was elucidated through the combination of STM experiments, high-resolution non-contact atomic force microscopy (nc-AFM) imaging, and DFT calculations. The additional STM experiments with different coverage of Se and different ratios of *m*TBPT to Se unravelled the critical role of Se concentration in stabilizing the C_{3h} conformer. The nc-AFM imaging (Fig. 3d) clearly resolved the C–Cu–C interlinking within the ordered networks and identified the presence of peripheral

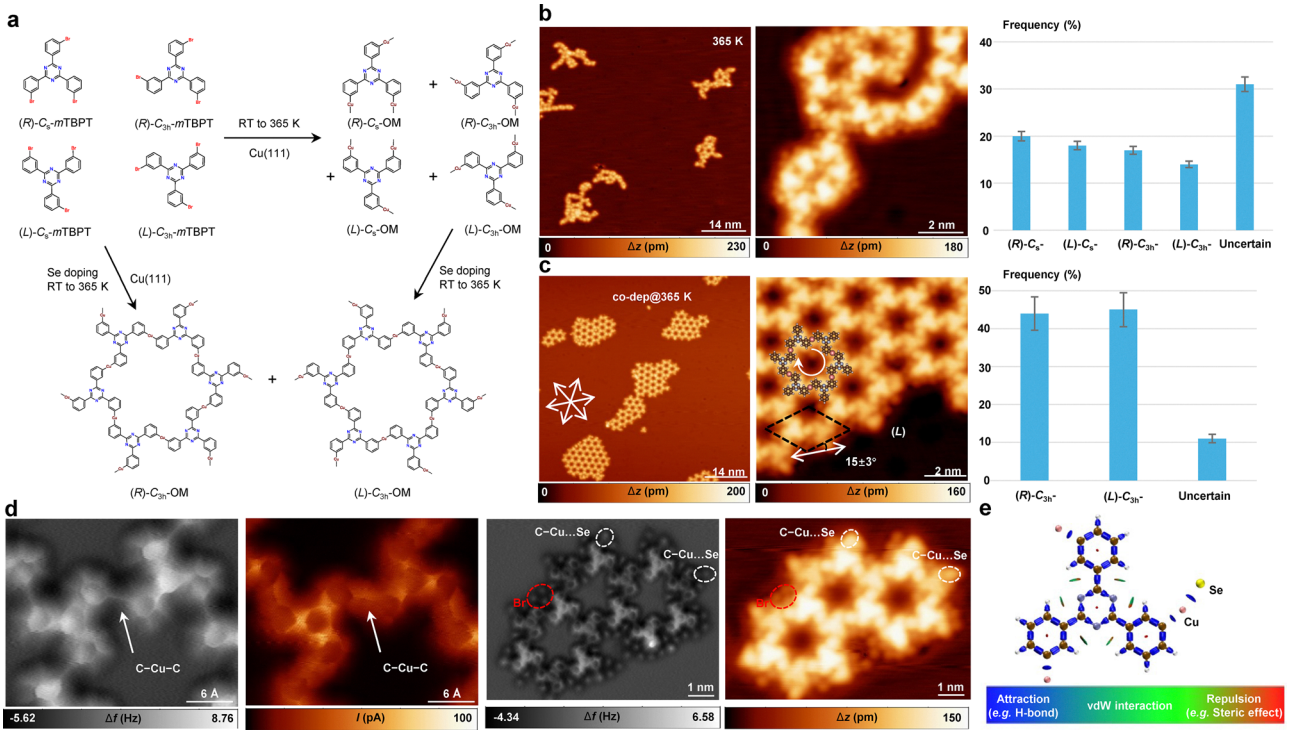

Fig. 3 (a) Reaction pathways of *m*TBPT precursors to random organometallics and crystalline 2D metal–organic networks after Se doping on Cu(111). (b) STM images depicting the random phase of C–Cu–C organometallics, and the corresponding statistical analysis with no obvious selectivity of C_s and C_{3h} conformers with (*R*) and (*L*) chirality. (c) STM images exhibiting the ordered organometallic networks formed by co-deposition of *m*TBPT and Se at 365 K, and the statistical analysis with high selectivity of C_{3h} moieties. (d) The nc-AFM frequency shift images and simultaneously acquired current images indicating the C–Cu–C interlinkings and the periphery C–Cu···Se interactions, respectively. (e) The IRI map of the finite C–Cu···Se moiety displaying the interactions between the Se atom and the C–Cu species. Reproduced from ref. 45. Copyright 2024 Nature Publishing Group.

C–Cu···Se interactions which were absent in the undoped nanostructures. These interactions were further supported by interaction region indicator (IRI) analysis (Fig. 3e), which revealed that Se atoms participated in weak yet significant noncovalent interactions with the C–Cu organometallic intermediates, effectively stabilizing the formed networks.

From the thermodynamic perspective, the energy barrier for the transformation of C_s to C_{3h} without Se was calculated to be 0.52 eV, which can be overcome at RT. The similar energy of C_s and C_{3h} conformers explains that the random OMs could be formed with no obvious selectivity. After Se doping, the transition barrier is decreased to 0.32 eV for the adjacent Se atoms helping to decouple the organic backbone from the surface and prevent hybridization. More importantly, the Se atom tends to couple to the C_{3h}–Cu species spontaneously with a quite shallow barrier, thus making the final state (FS) stable and the entire pathway exothermic by 0.58 eV. The Boltzmann ratio r is larger than 1 ($r \gg 1$) in quite a wide range of reaction temperature, where ΔE_1 is equal to 0.32 eV and ΔE_2 is equal to $\approx$0.58 eV, therefore the transformation from C_s to C_{3h} is preferred rather than the reverse transformation from C_{3h} to C_s after Se doping, and it accounts for the high selectivity of C_{3h} conformers after doping. Notably, the C_s–Cu···Se species (possible process before the initial state) were also considered and excluded owing to the reason that the overall energy of the C_{3h}–Cu network with peripheral C_{3h}–Cu···Se interactions was more stable compared to that of the C_s–Cu chain structure with terminal C_s–Cu···Se interactions.

This work demonstrated the precise conformational control in 2D MOF fabrication through Se doping and pioneered the possible combination of on-surface synthesis and the increased interest in selenides.

3.2. Disorder–order transition by selenium doping

In order to study the generality of the Se doping strategy and the effect of C–M–Ch bonding, Cai *et al.* presented a recent work using a much simpler and more general tripod precursor, 2,4,6-tris(4-bromophenyl)-1,3,5-triazine (*p*TBPT) on Cu(111), and achieved a disorder-to-order transition of 2D OM networks by Se doping at 360 K to 480 K, resulting in a more uniform network with ordered hexagonal OMs, as depicted in Fig. 4a.[46]

After sub-monolayer deposition of *p*TBPT on Cu(111) and annealing from RT to 480 K for 2 hours, the formed networks were structurally disordered, exhibiting a random distribution of polygons with mainly 4 to 8 edges. STM characterization, as shown in Fig. 4b, delineates the sample after annealing at 460 K, with part of the demetallized C–C interlinks indicated by blue ellipses. The statistical analysis in the right column of Fig. 4b exhibits the equivalent diameter distribution fitted with a Gaussian function, where the standard deviation is 0.61. Specifically, persistent homology (PH) methodology was implemented to provide topological quantification of the order in the

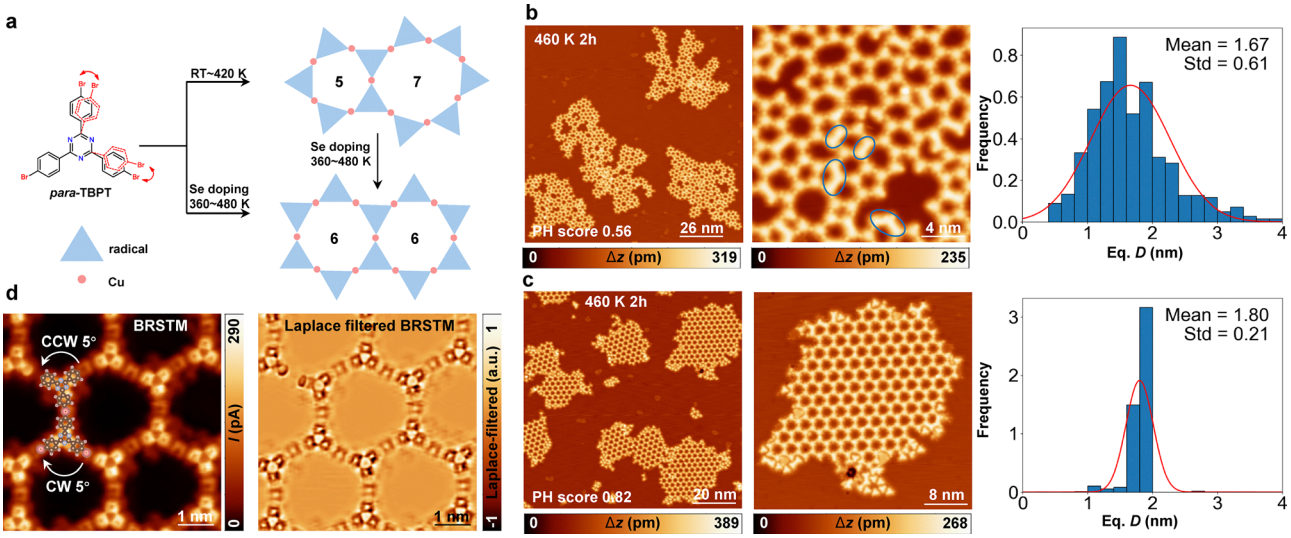

Fig. 4 (a) Reaction pathways of precursor *p*TBPT to organometallics with different membered rings and ordered hexagonal rings after Se doping on Cu(111). (b) STM images showing disordered porous organometallics with different membered rings formed after the deposition of *p*TBPT followed by annealing at 460 K for 2 h. (c) STM images depicting the honeycomb organometallic networks constructed by co-deposition of *p*TBPT and Se, followed by annealing at 460 K for 2 h. The right column in (b) and (c) indicates the distributions of the equivalent diameters, with the histograms fitted by the Gaussian function shown in red, which produce the mean values (Mean) and distributions (Std). (d) The constant-height current images before and after Laplace filtering of the honeycomb organometallic networks. Reproduced from ref. 46. Copyright 2025 Elsevier.

molecular networks.[71,72] The PH score of this disordered network is 0.56.

A striking contrast was also observed, as shown in Fig. 4c, with Se co-deposited under identical annealing conditions (460 K, 2 h). The STM images reveal well-ordered hexagonal OM networks. The corresponding pore size distribution (right column of Fig. 4c) demonstrates a significantly narrower Gaussian profile, indicating a much smaller standard deviation (only 0.21) and confirming the increased structural homogeneity induced by Se doping. The PH score increased to 0.82. The high-resolution STM image provides indirect evidence of the C–Cu···Se interaction in the periphery of the network.

BRSTM images before and after Laplace filtering in Fig. 4d demonstrated subtle rotational distortions within the building blocks of the hexagonal motifs, where the precursor moieties exhibited slight clockwise or counterclockwise rotations by 5°. Despite this, the overall network remains racemic and structurally homogeneous, highlighting the ability of Se doping to tolerate and accommodate residual molecular flexibility without compromising global order.

The Laplace filtered image distinctly resolves the molecular backbones and reveals the precise hexagonal arrangement of *p*TBPT interlinked with Cu adatoms. The BRSTM images provide direct evidence of the structural uniformity of the network.

Nudged elastic band (NEB) calculations illustrate that Se doping significantly reduces the energy barrier required for the transformation of non-hexagonal OM rings to hexagonal ones, from 0.76 eV to 0.20 eV. This barrier reduction enhances the thermodynamic accessibility of the ordered phase and enables the system to achieve high crystallinity within practical annealing times. This work not only demonstrated the generality of the Se doping strategy but also unraveled the distinct details in the transformation mechanisms and the effect of C–M–Ch bonding.

Conclusions and outlook

This paper mainly reviewed ChBIs on surfaces, including ChB with Se- and Te-substituted precursors, the Ch–organic interaction, and the C–M–Ch bonding through Se doping. The exploration of ChB has primarily focused on its role in directing molecular on-surface self-assembly, while the doping strategy has been demonstrated to effectively regulate conformationally flexible precursors, thereby enabling the formation of more ordered nanostructures during on-surface reactions. These findings enrich the existing toolbox of chemical on-surface science, for the design of much more ordered low-dimensional nanostructures and for future development in molecular electronics and crystal engineering.

The future applications of chalcogen atoms are highly promising. For example, the role of Se doping has extended beyond simple structural templating, exemplifying a broader principle in on-surface science where subtle adjustments in the chemical environment can decisively influence the outcome of on-surface synthesis processes. By actively modulating the energy landscape and stabilizing specific transition states, Se atoms serve as molecular directors that guide the system toward thermodynamically favored architectures. Future research studies may leverage this concept to explore other chalcogen dopants or combine heteroatoms to further refine control over conformational dynamics and topological selectivity. The ability to direct flexible precursors into specific ordered frameworks *via* doping opens new possibilities for the

programmable synthesis of functional 2D materials, MOFs and designer nanoporous networks with tailored electronic, optical and magnetic properties.

It is noteworthy that the doping effect of Se in on-surface synthesis may critically depend on the choice of the substrate. The regulatory effect of Se is largely attributed to the competition between the adsorption and intermolecular interactions on surfaces.[73–76] On inert surfaces, such as graphite, the lack of strong substrate interactions typically induces lower diffusion barriers for Se adatoms, which may result in even higher Se mobility.[77–79] Excessively high mobility is generally unfavourable in directing the ordered assembly of molecular networks, as Se adatoms may not be able to stabilize local structures.[80–82] The nature and surface parameters are crucial in the regulation of ChBIs involved nanostructures. Significantly, the protopolymer of an ordered OM network formed after Se doping does not yield highly ordered covalent nanostructures at elevated temperatures due to the energy barriers and the stability of final products. Milder activation methods, such as photoactivation, may be more effective than thermal activation with the aim to optimize the chalcogen doping strategy.

In summary, the regulation of low-dimensional nanostructures by chalcogen atoms, especially Se and Te, has proven to be an effective strategy for controlling molecular conformation, promoting structural order, and enabling precise on-surface self-assembly. The role of ChBIs offers valuable approaches for constructing ordered nanostructures. With some challenges coexisting, the exploration of chalcogen atoms remains an open and evolving field. Continued investigations into their diverse functions, doping behaviors, mechanisms and the combination of on-surface synthesis are expected.

Conflicts of interest

There are no conflicts to declare.

Data availability

No primary research results, software or code have been included and no new data were generated or analysed as part of this review.

Acknowledgements

L. C. and A. T. S. W. acknowledge financial support from the National Research Foundation Singapore (NRF-CRP26-2021RS0002).

References

1 J. V. Barth, G. Costantini and K. Kern, *Nature*, 2005, **437**, 671–679.
2 D. Wang, L. Wan and C. Bai, *Mater. Sci. Eng., R*, 2010, **70**, 169–187.
3 J. A. A. W. Elemans, S. Lei and S. De Feyter, *Angew. Chem., Int. Ed.*, 2009, **48**, 7298–7332.
4 Q. Shen, H. Gao and H. Fuchs, *Nano Today*, 2017, **13**, 77–96.
5 S. Clair and D. G. de Oteyza, *Chem. Rev.*, 2019, **119**, 4717–4776.
6 N. Wu, W. Shi, W. Wang and Y. Lei, *Small*, 2025, 2412780.
7 J. Cai, P. Ruffieux, R. Jaafar, M. Bieri, T. Braun, S. Blankenburg, M. Muoth, A. P. Seitsonen, M. Saleh, X. Feng, K. Müllen and R. Fasel, *Nature*, 2010, **466**, 470–473.
8 Q. Fan, J. M. Gottfried and J. Zhu, *Acc. Chem. Res.*, 2015, **48**, 2484–2494.
9 D. M. Packwood and T. Hitosugi, *Nat. Commun.*, 2018, **9**, 2469.
10 K. Gdula and D. Nieckarz, *J. Phys. Chem. C*, 2020, **124**, 20066–20078.
11 L. Lafferentz, F. Ample, H. Yu, S. Hecht, C. Joachim and L. Grill, *Science*, 2009, **323**, 1193–1197.
12 X. Liu, C. Guan, S. Ding, W. Wang, H. Yan, D. Wang and L. Wan, *J. Am. Chem. Soc.*, 2013, **135**, 10470–10474.
13 I. Piquero-Zulaica, J. Lobo-Checa, Z. M. Abd El-Fattah, J. E. Ortega, F. Klappenberger, W. Auwärter and J. V. Barth, *Rev. Mod. Phys.*, 2022, **94**, 045008.
14 Z. Chen, I. M. Grace, S. L. Woltering, L. Chen, A. Gee, J. Baugh, G. A. D. Briggs, L. Bogani, J. A. Mol, C. J. Lambert, H. L. Anderson and J. O. Thomas, *Nat. Nanotechnol.*, 2024, **19**, 986–992.
15 M. Kunitake and S. Uemura, *Chem. Lett.*, 2020, **49**, 565–573.
16 P. Hashizume, *e-J. Surf. Sci. Nanotechnol.*, 2023, **21**, 85–91.
17 N. Wu, M. Aapro, J. S. Jestilä, R. Drost, M. Martínez García, T. Torres, F. Xiang, N. Cao, Z. He, G. Bottari, P. Liljeroth and A. S. Foster, *J. Am. Chem. Soc.*, 2025, **147**, 1240–1250.
18 J. A. Theobald, N. S. Oxtoby, M. A. Phillips, N. R. Champnes and P. H. Beton, *Nature*, 2003, **424**, 1029–1031.
19 W. Yang, X. Chai, L. Chi, X. Liu, Y. Cao, R. Lu, Y. Jiang, X. Tang, H. Fuchs and T. Li, *Chem. – Eur. J.*, 1999, **5**, 1144–1149.
20 X. Ding, J. Chen and G. Ye, *Nat. Commun.*, 2024, **15**, 2782.
21 B. Jia, M. Enache, B. D. Gliemann, A. Jocic, M. Kivala and M. Stöhr, *Nanoscale Adv.*, 2025, **7**, 4897–4907.
22 N. Bilbao, I. Destoop, S. De Feyter and D. González-Rodríguez, *Angew. Chem., Int. Ed.*, 2016, **55**, 659–663.
23 Y. Liu, L. Wang, L. Zhao, Y. Zhang, Z. Li and F. Huang, *Chem. Soc. Rev.*, 2024, **53**, 1592–1623.
24 R. Gutzler, O. Ivasenko, C. Fu, J. L. Brusso, F. Rosei and D. F. Perepichka, *Chem. Commun.*, 2011, **47**, 9453–9455.
25 J. Shang, Y. Wang, M. Chen, J. Dai, X. Zhou, J. Kuttner, G. Hilt, X. Shao, J. M. Gottfried and K. Wu, *Nat. Chem.*, 2015, **7**, 389–393.
26 G. Gu, N. Li, X. Zhang, S. Hou, Y. Wang and K. Wu, *Acta Phys. Chim. Sin.*, 2016, **32**, 195–200.
27 J. Teyssandier, K. S. Mali and S. De Feyter, *ChemistryOpen*, 2020, **9**, 225–241.
28 R. Kampes, S. Zechel, M. D. Hager and U. S. Schubert, *Chem. Sci.*, 2021, **12**, 9275–9286.
29 J. Lawrence, G. C. Sosso, L. Đorđević, H. Pinfold, D. Bonifazi and G. Costantini, *Nat. Commun.*, 2020, **11**, 2103.

30 L. Xing, W. Jiang, Z. Huang, J. Liu, H. Song, W. Zhao, J. Dai, H. Zhu, Z. Wang, P. S. Weiss and K. Wu, *Chem. Mater.*, 2019, **31**, 3041–3048.
31 J. Eichhorn, T. Strunskus, A. Rastgoo-Lahrood, D. Samanta, M. Schmittel and M. Lackinger, *Chem. Commun.*, 2014, **50**, 7680–7682.
32 D. Barton, H. Gao, P. A. Held, A. Studer, H. Fuchs, N. L. Doltsinis and J. Neugebauer, *Chem. – Eur. J.*, 2017, **23**, 6190–6197.
33 M. Fritton, K. Otte, J. Björk, P. K. Biswas, W. M. Heckl, M. Schmittel and M. Lackinger, *Chem. Commun.*, 2018, **54**, 9745–9748.
34 J. A. Lipton-Duffin, O. Ivasenko, D. F. Perepichka and F. Rosei, Synthesis of Polyphenylene Molecular Wires by Surface-Confined Polymerization, *Small*, 2009, **5**, 592–597.
35 Q. Sun, C. Zhang, Z. Li, H. Kong, Q. Tan, A. Hu and W. Xu, *J. Am. Chem. Soc.*, 2013, **135**, 8448–8451.
36 Z. Wang, A. Hao and P. Xing, *Small*, 2024, **20**, 2407149.
37 X. Zhou and P. Xing, *Trends Chem.*, 2025, **7**, 460–473.
38 P. Politzer, J. S. Murray and T. Clark, *Phys. Chem. Chem. Phys.*, 2010, **12**, 7748–7757.
39 P. Politzer, J. S. Murray and T. Clark, *Phys. Chem. Chem. Phys.*, 2013, **15**, 11178–11189.
40 S. Scheiner, *Int. J. Quantum Chem.*, 2013, **113**, 1609–1620.
41 D. J. Pascoe, K. B. Ling and S. L. Cockroft, *J. Am. Chem. Soc.*, 2017, **139**, 15160–15167.
42 L. Chen, J. Xiang, Y. Zhao and Q. Yan, *J. Am. Chem. Soc.*, 2018, **140**, 7079–7082.
43 L. Camilli, C. Hogan, D. Romito, L. Persichetti, A. Caporale, M. Palummo, M. Di Giovannantonio and D. Bonifazi, *JACS Au*, 2024, **4**, 2115–2121.
44 F. Zheng, Q. Huang, J. Xiang, Z. Zhu, J. Lu, J. Xu, Z. Liang, L. Xie, F. Song and Q. Sun, *ACS Nano*, 2024, **18**, 28425–28432.
45 L. Cai, T. Gao and A. T. S. Wee, *Nat. Commun.*, 2024, **15**, 3235.
46 L. Cai, X. Zhang, J. Lu, J. Xiang, Q. Sun and A. T. S. Wee, *Chin. Chem. Lett.*, 2025, DOI: **10.1016/j.cclet.2025.111874**.
47 R. Hein and P. D. Bee, *Chem. Sci.*, 2022, **13**, 7098–7125.
48 R. Shi, Z. Wang, D. Yu, C. Wei, R. Qin and T. Mu, *Phys. Chem. Chem. Phys.*, 2024, **26**, 22593–22597.
49 Y. Xia, A. Hao and P. Xing, *ACS Nano*, 2023, **17**, 21993–22003.
50 R. Weiss, C. Schlierf and K. Schloter, *J. Am. Chem. Soc.*, 1976, **98**, 4668–4669.
51 H. Wang, B. Li, X. Wang, F. Yin, Q. Wei, X. Wang, Y. Ni and H. Wang, *Phys. Chem. Chem. Phys.*, 2023, **25**, 10836–10844.
52 L. Vogel, P. Wonner and S. M. Huber, *Angew. Chem., Int. Ed.*, 2019, **58**, 1880–1891.
53 N. Wintjes, J. Hornung, J. Lobo-Checa, T. Voigt, T. Samuely, C. Thilgen, M. Stöhr, F. Diederich and T. A. Jung, *Chem. – Eur. J.*, 2008, **14**, 5794–5802.
54 N. Biot and D. Bonifazi, *Chem. – Eur. J.*, 2020, **26**, 2904–2913.
55 Y. Ishigaki, K. Asai, H.-P. Jacquot de Rouville, T. Shimajiri, J. Hu, V. Heitz and T. Suzuki, *ChemPlusChem*, 2022, **87**, e202200075.
56 B. Ren, Y. Lu, R. Wang and H. Liu, *Chem. Phys.*, 2023, **565**, 111763.
57 S. Tsuzuki and N. Sato, *J. Phys. Chem. B*, 2013, **117**, 6849–6855.
58 M. Michalczyk, M. Malik, W. Zierkiewicz and S. Scheiner, *J. Phys. Chem. A*, 2021, **125**, 657–668.
59 G. Haberhauer and R. Gleiter, *Angew. Chem., Int. Ed.*, 2020, **59**, 21236–21243.
60 T. Steiner, *Angew. Chem., Int. Ed.*, 2002, **41**, 48–76.
61 A. A. Melekhova, A. S. Novikov, T. L. Panikorovskii, N. A. Bokach and V. Y. Kukushkin, *New J. Chem.*, 2017, **41**, 14557–14566.
62 P. Politzer, P. Lane, M. C. Concha, Y. Ma and J. S. Murray, *J. Mol. Model.*, 2007, **13**, 305–311.
63 A. Kühnle, *Curr. Opin. Colloid Interface Sci.*, 2009, **14**, 157–168.
64 C. A. Hunter, *Chem. Sci.*, 2013, **4**, 834–848.
65 B. Xu, J. Deng, X. Ding, J. Sun and J. Z. Liu, *npj Comput. Mater.*, 2022, **8**, 47.
66 M. Lackinger, *Chem. Commun.*, 2017, **53**, 7872–7885.
67 H. Walen, D. Liu, J. Oh, H. J. Yang, Y. Kim and P. A. Thiel, *Chem. Phys. Chem.*, 2016, **17**, 2137–2145.
68 J. Kim, J. Park and D. Ko, *Thin Solid Films*, 2018, **653**, 173–178.
69 A. F. Qasrawi and H. D. Aloushi, *Phys. B*, 2019, **569**, 62–67.
70 Z. Chen, T. Lin, H. Li, M. Sun, C. Su, B. Huang and K. Loh, *Nano Res.*, 2022, **15**, 2741–2745.
71 A. Gutierrez, M. Buchet and S. Clair, *Chem. Phys. Chem.*, 2019, **20**, 2286–2291.
72 J. Lu, D. Nieckarz, H. Jiang, Z. Zhu, Y. Yan, F. Zheng, W. Rżysko, J. Lisiecki, P. Szabelski and Q. Sun, *ACS Nano*, 2023, **17**, 20194–20202.
73 G. Vasseur, Y. Fagot-Revurat, M. Sicot, B. Kierren, L. Moreau, D. Malterre, L. Cardenas, G. Galeotti, J. Lipton-Duffin, F. Rosei, M. Di Giovannantonio, G. Contini, P. Le Fèvre, F. Bertran, L. Liang, V. Meunier and D. F. Perepichka, *Nat. Commun.*, 2016, **7**, 10235.
74 T. Wang and J. Zhu, *Surf. Sci. Rep.*, 2019, **74**, 97–140.
75 J. Dai, X. Zhao, Z. Peng, J. Li, Y. Lin, X. Wen, L. Xing, W. Zhao, J. Shang, Y. Wang, J. Liu and K. Wu, *J. Am. Chem. Soc.*, 2023, **145**, 13531–13536.
76 Z. Liang, S. Wu, J. Wang, Y. Qin, F. Cheng, L. Cao and H. Xu, *ACS Nano*, 2023, **17**, 10938–10946.
77 K. Nakada and A. Ishii, *Solid State Commun.*, 2011, **151**, 13–16.
78 T. K. Piskorz, C. Gobbo, S. J. Marrink, S. De Feyter, A. H. de Vries and J. H. van Esch, *J. Phys. Chem. C*, 2019, **123**, 17510–17520.
79 J. Jia, A. Bendounan, H. M. N. Kotresh, K. Chaouchi, F. Sirotti, S. Sampath and V. A. Esaulov, *J. Phys. Chem. C*, 2013, **117**, 9835–9842.
80 X. Wang, A. Chen, X. Wu, J. Zhang, J. Dong and L. Zhang, *Nano-Micro Lett.*, 2024, **16**, 163.
81 S. K. Yadav, A. Kumar and N. Mehta, *RSC Adv.*, 2023, **13**, 13564–13574.
82 R. Younas, G. Zhou and C. L. Hinkle, *Processes*, 2025, **13**, 791.